2009 IEEE International Conference on Robotics and Automation
Kobe International Conference Center
Kobe, Japan, May 12-17, 2009

A Harmonic Potential Field Approach for Navigating a Rigid, Nonholonomic Robot in a Cluttered Environment

Ahmad A. Masoud
Electrical Engineering Department, KFUPM, P.O. Box 287, Dhaharan 31261, Saudi Arabia, masoud@kfupm.edu.sa

Abstract: This paper demonstrates the ability of the harmonic potential field (HPF) planning approach to generate a provably-correct, constrained, well-behaved trajectory for a rigid, nonholonomic robot (a tractor-trailer robot is not rigid) in a stationary, cluttered environment. This is accomplished using a closed loop control scheme that is inspired by model predictive control (MPC). The scheme is realized using a synchronizing signal derived from the HPF along with a procedure for inverting the process the robot is using for actuating motion. Performance proofs as well as simulation results of the suggested planner are supplied.

I. Introduction and Background

A planner is an interface between an operator and a servo process whose function is to interpret the commands and constraints on the process within the confines of the environment which the process is situated in. Despite the diversity of planning methods [1,2] they may all be divided into two classes: a class that separates a planner into two modules one called the high level controller (HLC) and the other is called the low level controller (LLC). The first is responsible for converting the command, constraints and environment feed into a desired behavior which the process must find a way to actualize if the task is to be accomplished (a know-what-to-do guidance signal). On the other hand, the second module determines what actions the process actuators of motion should release in order to actualize the desired behavior (a know-how-to-do control signal). Although this division of role in building planners is widely accepted by researchers in the area, it is believed to be a source of several problems. It is well-known in practice that processes using the HLC-LLC paradigm are relatively slow. Incompatibilities between the guidance and control signals could lead to unwanted artifacts in the behavior and undesirable control effort that consumes too much energy or put too much strain on the actuators. Jointly designing the guidance and control modules should yield a simpler and more efficient planner compared to a design that treats the two modules separately.

Simultaneous consideration of the guidance and control signals in the design of a planner is a challenging task. While limited success was achieved in designing controllers that can incorporate simple avoidance regions with convex geometry in state-space [3,4], imposing nonconvex avoidance regions in the state-space of a dynamical system is difficult [5,6]. The task is further complicated when state-space constraints have to be implemented along with constraints in the control space as is the case with dynamical, nonholonomic systems. Instead of using the two-tier approach to planner design or the joint state-space control space approach, an approach in the middle is adopted. Here the capabilities of a carefully selected planner that can only generate a guidance signal (i.e. deals only with the kinematic aspects of motion) are augmented to generate also the needed control signal. The guidance field from the kinematic planner is left unchanged. However, instead of the control component of the planner being designed to enforce strict compliance of motion with the guidance field, we only require that the control component strongly discourages motion from deviating from the course set by the guidance field (effective compliance with guidance).

The extremely rich variety of kinematic motion planners may be categorized in one of two classes: path tracking planners and goal seeking planners. A path tracking planner provides a sequence of guidance instructions that mark one and only one path from an initial state to a target state. If an unexpected event occur throwing the state away from the guidance path, it must find its way back to the path in order to proceed to the target. On the other hand, a goal seeking planner supplies a guidance instruction at every possible state the system may exist in. Therefore, a disruption caused by an influence external to the system will not cause a halt in the effort to drive the state closer to the target.

The HPF approach is an excellent goal-seeking planner. It works by inducing, using a potential field, a dense collective of guidance vectors on the admissible space of the robot (Ω). A group structure is then evolved on this collective to generate a macro template encoding the guidance information the process needs to execute. The action selection mechanism the approach utilizes for generating the structure is in conformity with the artificial life (AL) method [7]. The HPF approach offers a solution to the local minima problem faced by the potential field approach Khatib suggested in [8]. It was simultaneously and independently proposed by several researchers [9-12] of whom the work of Sato in 1987 may be regarded as the first on the subject [13]. An HPF is generated using a Laplace boundary value problem (BVP) configured using a properly chosen set of boundary conditions. There are several settings one may use for a Laplce BVP (LBVP) in order to generate a navigation potential [14-16]. Each one of these settings possesses its own, distinct, topological properties [12]. An example is shown below of an LBVP that is configured using the homogeneous Neumann boundary conditions and encodes region avoidance constraints and target location:

$$\nabla^2 V(X) \equiv 0 \qquad X \in \Omega \tag{1}$$

subject to: $V(X_S) = 1$, $V(X_T) = 0$, and $\dfrac{\partial V}{\partial \mathbf{n}} = 0$ at $X = \Gamma$,

where Ω is the workspace, Γ is its boundary, $\mathbf{n}$ is a unit vector normal to Γ, X_s is the start point, and X_T is the target point. The trajectory (X(t)) is generated using the dynamical system:

$$\dot{X} = -\nabla V(X) \qquad X(0) = X_0 \in \Omega \tag{2}$$

The trajectory is guaranteed to:

1- $\lim_{t\to\infty} X(t) \to X_T$ 2- $X(t) \in \Omega \quad \forall \mathbf{t}$

Below is also a BVP similar to (1) that adds motion arrival orientation to the target to the set of encoded features:

$$\nabla^2 V(X) \equiv 0 \qquad X \in \Omega \tag{3}$$

subject to: $V(X_S) = 1, V(X_T) = 0, V(X_T + \epsilon \cdot \mathbf{h}) = 1$, $\dfrac{\partial V}{\partial \mathbf{n}} = 0$ at $X = \Gamma$,

where $1 >> \epsilon > 0$ and $\mathbf{h}$ is a unit vector in the target direction.

Harmonic functions have many useful properties[17] for motion planning. Most notably, a harmonic potential is also a Morse function [21] and a general form of the navigation function suggested in [18]. The HPF approach may be configured to operate in a model-based and/or sensor-based mode. It can also be made to accommodate a variety of constraints [16]. It ought to be mentioned that the HPF approach is only a special case of a much larger class of planners called: evolutionary, pde-ode motion planners [14]. Figures-1 shows the guidance fields and paths generated by a special type of HPF planners [16] called nonlinear, anisotropic HPF planner (NAHPF). In addition to enforcing regional avoidance constraints, NAHPF planners can also enforce directional constraints in Ω.

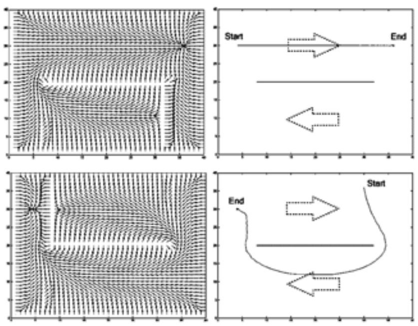

Figure-1: Output from a directional sensitive, kinematic, HPF planner.

Until now HPF planners can only deal with holonomic robots. In general, extending a holonomic planner to work under nonholonomic constraints is not always possible. However, due to the properties HPF planners enjoy, the situation is different. A planner for a nonholonomic robot whose points satisfy the rigidity constraints may be constructed by utilizing the gradient guidance field from an HPF as a motivator of motion. This requires that the nonholonomic robot be described using a two-stage model (figure-2). The first stage models the manner in which the robot converts the control variables used to actuate motion in its local coordinates. The second stage is concerned with transforming the motion from the local coordinates into one that is global coordinates-centered (namely, position and orientation).

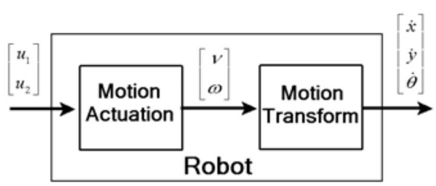

Figure-2: Two-stage model of a rigid, nonholonomic robot.

The nonholonomic planner is constructed as follows: at each point in Ω (X_i) a reference motion $dXr_i(X_i)/dt$ is selected as the negative gradient of the HPF. It is required that the robot's motion in its local coordinates be equal to the reference motion. To achieve this, an inverse of the motion actuation stage of the robot is applied to the field of reference motions. The field of reference motions marks the solution trajectories which the robot can proceed along to the target. The inverse process, in effect, attaches to each solution trajectory a dense sequence of control vectors. Due to limitations on the inversion process and (or) the initial state the robot is in, the robot will not remain on the solution trajectory it is currently situated at and will transit to a new one. In a manner similar to MPC [22], the robot will only use the first control instruction in the sequence associated with a solution trajectory and discard the remaining ones. This is repeated till the robot finally reaches its target (figure-3). This paper demonstrates that the above paradigm does provide good basis for building a provably-correct nonholonomic motion planner for rigid robots. It ought to be mentioned that the nature of the paradigm does not limit the construction of planners for planar robots and makes it possible to deal with three dimensional even N-D spaces

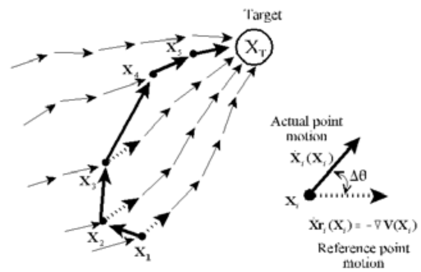

Figure-3: The MPC paradigm for the nonholonomic planner.

In section II the suggested HPF-based, nonholonomic controller for a massless robot is presented. Section III provides performance analysis for the massless controller. Section IV suggests an extension to the second order dynamics case. Simulation results are in section V and conclusions are in section VI.

II. The Kinematic Planner

Adapting the above approach to planning hinges on the ability to find a realization that can make the nonholonomic path of the robot as close as possible to the holonomic path generated by the gradient of an HPF. Achieving this, ensures that all the provably-correct properties of a path generated by a holonomic HPF planner are migrated to the corresponding nonholonomic path. A realization that can accomplish the above has two stages (figure-4): a stage that generates an HPF-based, synchronizing signal that attempts to align the velocity vector of the robot with the reference velocity vector selected as the negative gradient of the HPF. This synchronizing signal has the form:

$$\begin{bmatrix} \nu_r \\ \Delta\theta \end{bmatrix} = \begin{bmatrix} |-\nabla V| \cdot \cos^{\alpha}(\theta - \arg(-\nabla V)) \\ \arg(-\nabla V) - \theta \end{bmatrix} \tag{4}$$

where α is a non-negative integer, θ is the orientation of the robot in its world coordinates, Δθ is the difference between the orientation of the robot and the desired one and ν_r is the reference radial speed the robot is required to assume. The second stage operates on the synchronizing signal in (4) with an operator that attempts to invert the motion actuation process of the robot in order to yield the control signal $u=[u_1\ u_2]^T$:

$$\begin{bmatrix} u_1 \\ u_2 \end{bmatrix} = F\left(\begin{bmatrix} \nu \\ \Delta\theta \end{bmatrix}\right) \tag{5}$$

where F is an inverse operator (linear or nonlinear) derived from the motion actuation stage of the robot's model.

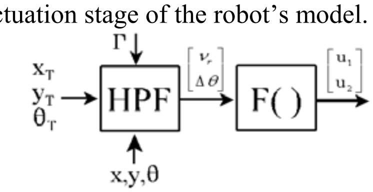

Figure-4: the nonholonomic planner - The massless case.

Below are the two-stage models and the inverse operator for two popular mobile robots, the differential drive robot and the front wheel steered car (the slow steering case):

1- The differential drive robot (DDR) (figure-5A):

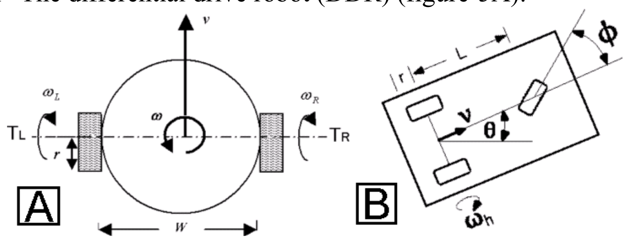

Figure-5: A-DDR mobile robot, B-FSR mobile robot.

The equations describing motion for such a robot are:

$$\begin{bmatrix}\dot{\mathbf{x}}\\ \dot{\mathbf{y}}\\ \dot{\theta}\end{bmatrix}=\begin{bmatrix}\cos(\theta) & \mathbf{0}\\ \sin(\theta) & \mathbf{0}\\ \mathbf{0} & \mathbf{1}\end{bmatrix}\begin{bmatrix}\nu\\ \omega\end{bmatrix} \quad (6), \qquad \begin{bmatrix}\nu\\ \omega\end{bmatrix}=\begin{bmatrix}\frac{\mathrm{r}}{2} & \frac{\mathrm{r}}{2}\\ \frac{\mathrm{r}}{\mathrm{W}} & \frac{-\mathrm{r}}{\mathrm{W}}\end{bmatrix}\begin{bmatrix}\omega_{\mathbf{R}}\\ \omega_{\mathbf{L}}\end{bmatrix} \quad (7)$$

where r is the radius of the robot's wheels, W is the width of the robot, ω_R and ω_L are the angular speeds of the right and left wheels of the robot respectively. The inverse operator is:

$$\begin{bmatrix}\omega_{\mathbf{R}}\\ \omega_{\mathbf{L}}\end{bmatrix}=\begin{bmatrix}\frac{1}{\mathrm{r}} & \frac{\mathrm{W}}{2\mathrm{r}}\\ \frac{1}{\mathrm{r}} & \frac{-\mathrm{W}}{2\mathrm{r}}\end{bmatrix}\begin{bmatrix}\nu_r\\ \Delta\theta\end{bmatrix} \quad (8)$$

2-The Front wheel Steered Robot (FSR) (figure-5B): The equations describing motion for this robot are:

$$\begin{bmatrix}\dot{\mathbf{x}}\\ \dot{\mathbf{y}}\\ \dot{\theta}\end{bmatrix}=\begin{bmatrix}\cos(\theta) & \mathbf{0}\\ \sin(\theta) & \mathbf{0}\\ \mathbf{0} & \mathbf{1}\end{bmatrix}\begin{bmatrix}\nu\\ \omega\end{bmatrix}, \quad \begin{bmatrix}\nu\\ \omega\end{bmatrix}=\begin{bmatrix}\mathrm{r}\cdot\omega_{\mathbf{h}}\\ \mathrm{r}\cdot\mathrm{L}\cdot\omega_{\mathbf{h}}\cdot\tan(\varphi)\end{bmatrix} \quad (9)$$

where L is the normal distance between the center of the front wheel and the line connecting the rear wheels, ω_h is angular speed of the rear wheels, and ϕ is the steering angle of the front wheel ($\pi/2>\phi>-\pi/2$). The inverse operator is:

$$\begin{bmatrix}\omega_h\\ \phi\end{bmatrix}=\begin{bmatrix}\nu_r\\ \tan^{-1}(\Delta\theta/(\mathrm{L}\cdot\nu_r))\end{bmatrix}. \quad (10)$$

In the above cases, it is possible to perfectly invert the actuation stage. If this is not possible, the pseudo inverse approach may be used to construct the inversion operator F. The equation of motion for many nonholonomic mobile robots may be written as:

$$\begin{bmatrix}\dot{\mathrm{x}}\\ \dot{\mathrm{y}}\\ \dot{\theta}\end{bmatrix}=\mathbf{G}(\mathrm{x},\mathrm{y},\theta,\nu,\omega) \quad (11)$$

where G is a nonlinear vector function. At a certain (x,y) point in space, equation-11 may be linearized at the current operating condition and the motion of the robot described as:

$$\begin{bmatrix}\dot{\mathrm{x}}\\ \dot{\mathrm{y}}\\ \dot{\theta}\end{bmatrix}=\begin{bmatrix}\cos(\theta) & 0\\ \sin(\theta) & 0\\ 0 & 1\end{bmatrix}\begin{bmatrix}\nu\\ \omega\end{bmatrix} \quad (12)$$

$$\begin{bmatrix}\nu\\ \omega\end{bmatrix}=\mathbf{A}(\mathrm{x},\mathrm{y},\theta)\begin{bmatrix}\mathrm{u}_1\\ \mathrm{u}_2\end{bmatrix} \quad (13)$$

where **A** need not necessarily be full rank. In this case the inverse operator may be constructed as:

$$\begin{bmatrix}\mathrm{u}_1\\ \mathrm{u}_2\end{bmatrix}=\mathbf{A}^+(\mathbf{x},\mathbf{y},\theta)\begin{bmatrix}\nu_r\\ \Delta\theta\end{bmatrix} \quad (14)$$

$\mathbf{A}^+$ is the pseudo inverse of **A** [23] and A is derived from **G**.

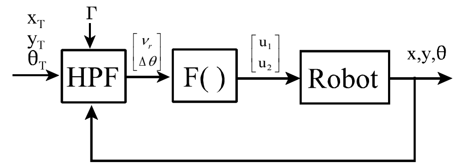

Figure-6: The close loop, HPF-based, nonholonomic system.

III. Performance Analysis

In this section two properties of the above controller are proven. It is shown that the closed loop system in figure-6 is stable for a general rigid nonholonomic robot. For the specific cases of the differential drive and front wheel steered robots, where perfect actuator inversion is possible, convergence to the target position and orientation is guaranteed. It is also proven that the trajectory of the robot can be made arbitrarily close to the trajectory laid by the gradient dynamical system directly derived from the HPF. This proves that the robot trajectory also satisfies all the provably-correct properties of a holonomic HPF path.

The proofs of closed loop stability assume that the pseudo inverse is used in constructing the inverse operator of the actuators. Proofs for this case subsumes the proofs for the cases where actuators inversion is perfect.

Proposition-1:A matrix **P** constructed as the product of a matrix **A** by its pseudo inverse ($\mathbf{P}=\mathbf{A}^+\mathbf{A}$) is positive semi-definite (**A** is not full-rank).

Proof: by definition the pseudo inverse of A is:

$$\mathbf{A}^+=\lim_{\delta\to 0}(\mathbf{A}^{\mathbf{T}}\mathbf{A}+\delta\cdot\mathbf{I})^{-1}\mathbf{A}^{\mathbf{T}}=\lim_{\delta\to 0}\mathbf{A}^{\mathbf{T}}(\mathbf{A}^{\mathbf{T}}\mathbf{A}+\delta\cdot\mathbf{I})^{-1}. \quad (15)$$

Let $\mathbf{Q}=\mathbf{A}^{\mathbf{T}}\mathbf{A}$, and $\mathbf{Z}=\delta\cdot\mathbf{I}$. Since **Q** is symmetric and **Z** is positive definite, they may be jointly diagonalizable [24] into:

$$\mathbf{Q}=\mathbf{U}^{\mathbf{T}}\mathbf{\Lambda}\mathbf{U} \text{ and } \mathbf{Z}=\mathbf{U}^{\mathbf{T}}\mathbf{U}, \quad (16)$$

where **U** is an orthonormal matrix and $\mathbf{\Lambda}$ is a diagonal matrix containing the eigenvalues of **Q** (λ_i). Substituting (16) into (15) in order to compute **P** we have:

$$\mathbf{P}=\lim_{\delta\to 0}(\mathbf{U}^{\mathbf{T}}\mathbf{U}+\mathbf{U}^{\mathbf{T}}\Lambda\mathbf{U})^{-1}\mathbf{U}^{\mathbf{T}}\Lambda\mathbf{U}=\lim_{\delta\to 0}[\mathbf{U}^{\mathrm{T}}(\mathbf{I}+\Lambda)^{-1}\Lambda\mathbf{U}] \quad (17)$$

$$=\lim_{\delta\to 0}[\mathbf{U}^{\mathrm{T}}\begin{bmatrix}\frac{\lambda_1}{1+\lambda_1} & 0 & \cdot & 0\\ 0 & \frac{\lambda_2}{1+\lambda_2} & \cdot & 0\\ \cdot & \cdot & \cdot & \cdot\\ 0 & \cdot & 0 & \frac{\lambda_N}{1+\lambda_N}\end{bmatrix}\mathbf{U}].$$

Since **Q** is constructed as the product of a matrix by its transpose, its eigenvalues are non-negative. Therefore, the eigenvalues of **P** lie in the interval [0,1), i.e. they are non-negative. Therefore **P** is positive semi-definite.

Proposition-2: The closed loop system constructed by using the control law in (14) with the system in (12,13) is stable. If **A** is full rank, then the robot will converge to the target position and orientation.

Proof: Consider the Liapunov function candidate:

$$\Xi=\mathrm{V}(\mathrm{x},\mathrm{y})+\frac{1}{2}(\Delta\theta)^{\mathbf{2}} \quad (18)$$

note that the HPF V is a Liapunov function that is positive everywhere in Ω except at $x=x_T$ and $y=y_T$ where it is equal to zero[16]. The derivative of Ξ with respect to time is:

$$\dot{\Xi}=\nabla\mathrm{V}\begin{bmatrix}\dot{\mathrm{x}}\\ \dot{\mathrm{y}}\end{bmatrix}-\Delta\theta\cdot\dot{\theta} \quad (19)$$

Manipulating (12), (13) and (14) we obtain:

$$\begin{bmatrix}\dot{x}\\ \dot{y}\\ \dot{\theta}\end{bmatrix}=\begin{bmatrix}\cos(\theta) & 0\\ \sin(\theta) & 0\\ 0 & 1\end{bmatrix}\mathrm{P}\begin{bmatrix}\cos^{\alpha}(\theta)\left|-\nabla \mathrm{V}\right|\\ \Delta\theta\end{bmatrix} \tag{20}$$

where $\mathbf{P}=\mathbf{AA}^{+}$. Substituting (20) in (19) we get:

$$\dot{\Xi}=\nabla\mathrm{V}\begin{bmatrix}\cos(\theta) & 0\\ \sin(\theta) & 0\end{bmatrix}\mathbf{P}\begin{bmatrix}\cos^{\alpha}(\Delta\theta)\left|-\nabla\mathbf{V}\right|\\ -\Delta\theta\end{bmatrix}+\begin{bmatrix}0 & \Delta\theta\end{bmatrix}\mathbf{P}\begin{bmatrix}\cos^{\alpha}(\Delta\theta)\left|-\nabla\mathbf{V}\right|\\ -\Delta\theta\end{bmatrix}. \tag{21}$$

The gradient of V may be expressed as:

$$\nabla\mathrm{V}=\left|\nabla\mathrm{V}\right|\cdot\begin{bmatrix}\cos(\arg(-\nabla\mathrm{V})+\pi)\\ \sin(\arg(-\nabla\mathrm{V})+\pi)\end{bmatrix} \tag{22}$$

substituting (22) into (21) we have:

$$\dot{\Xi}=\begin{bmatrix}-\left|\nabla\mathrm{V}\right|\cdot\cos(\Delta\theta) & 0\end{bmatrix}\mathbf{P}\begin{bmatrix}\cos^{\alpha}(\Delta\theta)\left|-\nabla\mathrm{V}\right|\\ -\Delta\theta\end{bmatrix}+\begin{bmatrix}0 & \Delta\theta\end{bmatrix}\mathbf{P}\begin{bmatrix}\cos^{\alpha}(\Delta\theta)\left|-\nabla\mathrm{V}\right|\\ -\Delta\theta\end{bmatrix} \tag{23}$$

or $\dot{\Xi}=-\begin{bmatrix}\left|\nabla\mathrm{V}\right|\cdot\cos(\Delta\theta) & \Delta\theta\end{bmatrix}\mathbf{S}\begin{bmatrix}\cos^{\alpha}(\Delta\theta)\left|-\nabla\mathrm{V}\right|\\ \Delta\theta\end{bmatrix}$, $\mathbf{S}=\mathbf{P}\begin{bmatrix}\cos^{\alpha-1}(\Delta\theta) & \mathbf{0}\\ \mathbf{0} & \mathbf{1}\end{bmatrix}$. (24)

There are two cases one for α even and the other for α odd. If α is odd, $\cos^{\alpha-1}(\Delta\theta)$ is non-negative for any value of Δθ. Since **P** is positive semidefinite, it can be shown by direct computation of the eigenvalues of **S** that the eigen values of **S** are non-negative provided that **P** is positive semidefinite. In other words, **S** is also positive semidefinite. For the case where perfect inversion of the motion actuation process is possible (i.e. **P=I**), (24) is zero at $|\nabla V|=0$, $\Delta\theta=0$ and $\Delta\theta=\pi/2$. Equation (4) may be used to compute the minimum invariant set of the system: $|\nabla V|=0$, $\Delta\theta=0$ to which the robot will converge. Since it is proven that an HPF is Morse [21] convergence of $|\nabla V|$ to zero implies convergence of x and y to x_T and y_T. Also convergence of Δθ to zero implies that the robot will converge to the orientation encoded by the HPF at x_T and y_T. For the case where actuator inversion is not perfect (i.e. **P≠I**), convergence analysis will depend on the structure of **P**. However, from the above it can be easily sown that this will only cause deadlock. For the case where α is even, the sign of $\cos^{\alpha-1}(\Delta\theta)$ is negative for $|\Delta\theta|>\pi/2$. However from (4) it can be shown that : $\lim_{\mathbf{t}\to\infty}\theta(\mathbf{t})\to\arg(-\nabla\mathrm{V})$. (25)

In other words, $\Delta\theta\to 0$ and S is negative semidefinite.

Proposition-3: Let ρ be the spatial projection of the trajectory X(t) laid by the gradient dynamical system in (2). Also let ρ_n be the spatial projection of the trajectory laid by the suggested nonholonomic planner (figure-7). Let δ(t) be the deviation between ρ and ρ_n at time t. Let δ_m be the maximum deviation. If the motion actuation process is fully invertible, then by setting α high enough, δ_m may be made arbitrarily small,

$$\lim_{\alpha\to\infty}\delta_{\mathbf{m}}\to 0.$$

Proof: Let **e** be a unit vector normal to $-\nabla V$,

$$\mathbf{e}=\begin{bmatrix}\sin(\arg(-\nabla\mathrm{V}))\\ -\cos(\arg(-\nabla\mathrm{V}))\end{bmatrix}. \tag{26}$$

The rate of change of δ(t) may be computed as:

$$\dot{\delta}=\mathbf{e}^{\mathbf{T}}\begin{bmatrix}\dot{x}\\ \dot{y}\end{bmatrix}=\mathbf{e}^{\mathbf{T}}\begin{bmatrix}\cos(\theta) & \mathbf{0}\\ \sin(\theta) & \mathbf{0}\end{bmatrix}\begin{bmatrix}\cos^{\alpha}(\Delta\theta)\left|-\nabla\mathrm{V}\right|\\ \Delta\theta\end{bmatrix} \tag{27}$$

$$=-\left|-\nabla\mathrm{V}\right|\cdot\sin(\Delta\theta)\cos^{\alpha}(\Delta\theta).$$

The maximum of the above is achieved at:

$$\Delta\theta=\cos^{-1}\left(\sqrt{\frac{\alpha}{1+\alpha}}\right)` \tag{28}$$

Since V is harmonic, $\quad |\nabla V|\le C_m \qquad x,y\in\Omega$ (29)

where C_m is a finite positive constant [25]. A upper bound on dδ/dt (δd_m) may be constructed as:

$$\delta\mathrm{d}_{\mathrm{m}}\le\mathrm{C}_{\mathrm{m}}\cdot\frac{\alpha^{\alpha}}{(1+\alpha)^{1+\alpha}} \tag{30}$$

As can be seen, the rate of change in δ tends to zero as α goes to infinity. Since the system is stable, we have:

$$\delta(0)=0,\quad \lim_{\mathbf{t}\to\infty}\delta(0)\to 0,$$
$$\lim_{\mathbf{t}\to\infty}\dot{\delta}(\infty)\to 0,\ \text{and}\ \int_{\mathbf{0}}^{\infty}\dot{\delta}(\mathrm{t})\mathrm{dt}=0\,. \tag{31}$$

Since (27) satisfies the Lipschitz conditon and its convergence to zero is independent of α and depends mainly on (4), an upper bound on δ_m may be constructed as follow:

$$\dot{\delta}=\begin{cases}0 & 0\ge\mathrm{t}\\ +\delta\mathrm{d}_{\mathrm{m}} & \mathrm{T}/2\ge\mathrm{t}>0\\ -\delta\mathrm{d}_{\mathrm{m}} & \mathrm{T}\ge\mathrm{t}>\mathrm{T}/2\text{'}\\ 0 & \mathrm{t}>\mathrm{T}\end{cases} \tag{32}$$

where T is the effective time dδ/dt converges to zero. Using the above the maximum deviation may be bounded as:

$$\delta m\le\delta d_m\cdot T/2 \tag{33}$$

which also tends to zero as α becomes very large.

Proving that the deviation between the trajectory generated directly from the gradient of the HPF and the nonholonomic path may be driven to zero. This in turn implies that the nonholonomic path inherits all the provably-correct properties of the gradient, this includes obstacle avoidance.

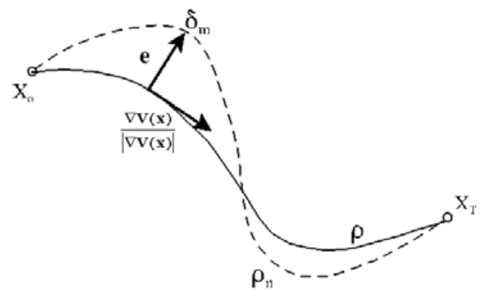

Figure-7: deviation between the HPF trajectory and the nonholonomic trajectory.

IV. A Suggested Extension: The Kinodynamic Case

The dynamic behavior of the differential drive robot that ties the torques applied to the right and left wheels (T_R, T_L) to the position and orientation of the robot may be described using two, coupled differential equations. The first one is obtained by differentiating (6) with respect to time,

$$\begin{bmatrix}\ddot{x}\\ \ddot{y}\\ \ddot{\theta}\end{bmatrix}=\begin{bmatrix}\cos(\theta) & \mathbf{0}\\ \sin(\theta) & \mathbf{0}\\ \mathbf{0} & \mathbf{1}\end{bmatrix}\begin{bmatrix}\dot{\nu}\\ \dot{\omega}\end{bmatrix}+\begin{bmatrix}-\sin(\theta)\dot{\theta} & \mathbf{0}\\ \cos(\theta)\dot{\theta} & \mathbf{0}\\ \mathbf{0} & \mathbf{0}\end{bmatrix}\begin{bmatrix}\nu\\ \omega\end{bmatrix}, \tag{34}$$

and the second is derived using Lagrange dynamics in the natural coordinates of the robot,

$$\begin{bmatrix}\dot{\nu}\\ \dot{\omega}\end{bmatrix}=\frac{1}{\mathrm{M}}\begin{bmatrix}\frac{1}{\mathrm{r}} & \frac{1}{\mathrm{r}}\\ \frac{-4\cdot\mathrm{r}}{\mathrm{W}^{3}} & \frac{4\cdot\mathrm{r}}{\mathrm{W}^{3}}\end{bmatrix}\begin{bmatrix}\mathrm{T_R}\\ \mathrm{T_L}\end{bmatrix}=\mathrm{B}\cdot\begin{bmatrix}\mathrm{T_R}\\ \mathrm{T_L}\end{bmatrix} \tag{35}$$

Where M is the mass of the robot. It can be demonstrated by simulation that using the control scheme for a massless robot with robots that have mass will cause instability. To stabilize the system an omni-directional, linear viscous dampening force applied in the natural coordinates of the robot is used to generate the control signal:

$$\begin{bmatrix} T_R \\ T_L \end{bmatrix} = \mathbf{B}^{-1} \cdot \left[K_P \cdot \begin{bmatrix} |-\nabla V| \cdot \cos^{\alpha}(\arg(-\nabla V) - \theta) \\ \arg(-\nabla V) - \theta \end{bmatrix} - K_d \cdot \begin{bmatrix} \dot{\rho} \\ \dot{\theta} \end{bmatrix} \right], \quad (36)$$

where K_P and K_D are positive constants, $\mathbf{B}^{-1}$ is the inverse of $\mathbf{B}$, and $\dot{\rho}$ is the radial speed of the robot,

$$\dot{\rho} = \sqrt{\dot{x}^2 + \dot{y}^2}\,. \quad (37)$$

The block diagram of the planner is shown in figure-8.

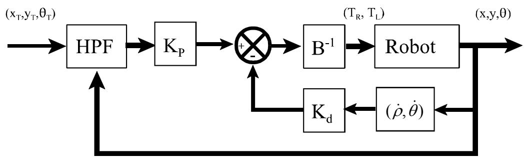

Figure-8: A dynamic, HPF-based planner, nonholonomic case.

Rate feedback in the natural coordinates of the robot is needed to stabilize the response and make the system yield to the guidance signal derived from the HPF. Significant transients are expected for a small coefficient of rate feedback. Although increasing this coefficient reduces the transients, it results in reducing the speed of the robot. One way to cope with this problem is to sensitize the damping to the guidance signal is to notice that changing the speed of the robot is not needed if the actual speed of the system is equal to the reference speed. This is realizd using the control signal:

$$\begin{bmatrix} T_R \\ T_L \end{bmatrix} = \mathbf{B}^{-1} \cdot [K_P \cdot \begin{bmatrix} |-\nabla V| \cdot \cos^{\alpha}(\arg(-\nabla V) - \theta) \\ 0 \end{bmatrix} - K_d \cdot \begin{bmatrix} \dot{\rho} \\ \dot{\theta} - (\arg(-\nabla V) - \theta) \end{bmatrix}] \quad (38)$$

It was proven in [16] that the gradient dynamical system in (2) which is constructed from an underlying harmonic potential guarantees convergence from any point in Ω to a specified target point. The proof makes use of the fact that a harmonic potential is also a Liapunov function candidate. The following proposition shows that the procedure suggested in (38) makes it possible for the dynamical system in (2) to steer a differential drive robot with second order dynamics from any initial position and orientation in Ω to the target position and orientation encoded in the harmonic field V. The LaSalle invariance principle [26], is used in the proof.

Propositon-4: The control law in (38) applied to a differential drive robot with second order dynamics described by the system equation in (34,35) guarantees global asymptotic convergence of the robot from any initial position and orientation in Ω to the target potion point (x_T, y_T) and orientation $(\arg(-\nabla V(x_T, y_T))$ encoded in the harmonic potential V provided that Kp>0 and Kd>0.

Proof: consider the following Liapunov function candidate:

$$\Xi = K_P \cdot M \cdot V(x,y) + \frac{1}{2} K_d \cdot I \cdot (\arg(-\nabla V(x,y) - \theta)^2 + \frac{1}{2} I \cdot \dot{\theta}^2 + \frac{1}{2} M \cdot \dot{\rho}^2 \quad (39)$$

where M is the mass of the robot, I is its inertia , K_p and K_d are positive constants. Notice that V(x,y) is a valid liapunov function [16]. It is always positive except at the target point (x_T, y_T) where it is equal to zero. As a result Ξ is always positive except at the target position and orientation when the robot is at a standstill. The time derivative of Ξ is:

$$\begin{aligned} \dot{\Xi} = {} & K_P \cdot M \cdot \nabla V(x,y)^T \begin{bmatrix} \dot{x} \\ \dot{y} \end{bmatrix} - K_d \cdot I \cdot \dot{\theta} \cdot (\arg(-\nabla V(x,y)) - \theta) \\ & + I \cdot \dot{\theta} \cdot \ddot{\theta} + M \cdot \dot{\rho} \cdot \ddot{\rho} \end{aligned} \quad (40)$$

Notice that: $$\nabla V(x,y) = |\nabla V(x,y)| \begin{bmatrix} \cos(\arg(-\nabla V(x,y)) + \pi) \\ \sin(\arg(-\nabla V(x,y)) + \pi) \end{bmatrix} \quad (41)$$

and $$\begin{bmatrix} \dot{x} \\ \dot{y} \end{bmatrix} = \dot{\rho} \begin{bmatrix} \cos(\theta) \\ \sin(\theta) \end{bmatrix}. \quad (42)$$

Substituting (35), (38), (41) and (42) in (40) and noticing that for a differential drive robot **B+=B^-1^,** we have:

$$\begin{aligned} \dot{\Xi} = {} & -K_P \cdot M \cdot \dot{\rho} \cdot |\nabla V(x,y)| \cdot \cos(\arg(-\nabla V(x,y)) - \theta) \\ & - K_d \cdot I \cdot \dot{\theta} \cdot (\arg(-\nabla V(x,y)) - \theta) - K_d \cdot I \cdot \dot{\theta}^2 \\ & - K_P M \cdot \dot{\rho}^2 + K_d \cdot I \cdot \dot{\theta} \cdot (\arg(-\nabla V(x,y)) - \theta) \\ & + K_P \cdot M \cdot \dot{\rho} \cdot |\nabla V(x,y)| \cdot \cos(\arg(-\nabla V(x,y)) - \theta) \end{aligned} \quad (43)$$

Therefore: $$\dot{\Xi} = -K_d \cdot I \cdot \dot{\theta}^2 - K_P M \cdot \dot{\rho}^2\,. \quad (44)$$

As can be seen the time derivative of the Liapunov function is negative semi-definite. According to LaSalle principle motion will converge to a subset of the set of points (E) for which the time derivative of Ξ is zero:

$$E = \{\dot{\rho} = 0,\ \dot{\theta} = 0,\ x,\ y,\ \theta\}. \quad (45)$$

The subset is called the minimum invariant set (W) and may be computed as the set of point for which the gradient dynamical system in (2). It was shown in [16] that motion for (2) is guaranteed to converge to the target point x_T, y_T , hence the orientation of the robot will converge to $\arg(-\nabla V(x_T, y_T))$. The dynamical differential drive robot will converge to set:

$$W = \{\dot{\rho} = 0,\ \dot{\theta} = 0,\ x = x_T,\ y = y_T,\ \theta = \arg(-\nabla V(x_T, y_T)\} \quad (46)$$

provided that K_p and K_d are positive.

V. Simulation Results

The suggested controller is tested for the massless case using the gradient guidance field in figure-9. This field encodes the simple behavior of move right and stay at the center.The trajectories obtained for different values of α are shown in figure-10. The simulation is carried out for both the differential drive robot and the front wheel-steered robot. The time step ΔT=.01 second and the total duration of the stimulation is 6 seconds. The trajectories obtained for both robots are identical. The control signal for both robots (θ(0)=π/2 and α=9) are shown in figure- 11A for the DDR and figure-11B for the FSR.

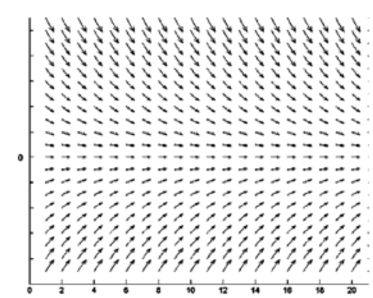

Figure-9: Move right and stay at center gradient guidance field.

The controller designed for the massless case fails when used with a differential drive robot with a mass. Direct use of the guidance force as a control signal will cause instability. To stabilize the system an omni-directional, linear viscous dampening force applied in the natural coordinates of the robot is used to generate the control signal. The response of the system is shown in figure-12 for K_P=.001, K_d=30 and an α=0. As can be seen, the use of rate feedback in the natural coordinates of the robot did stabilize the response and made the system yield to the guidance signal derived from the HPF. Significant transients are observed for a small coefficient of rate feedback. Although increasing this coefficient reduces the transients, it results in reducing the speed of the robot.

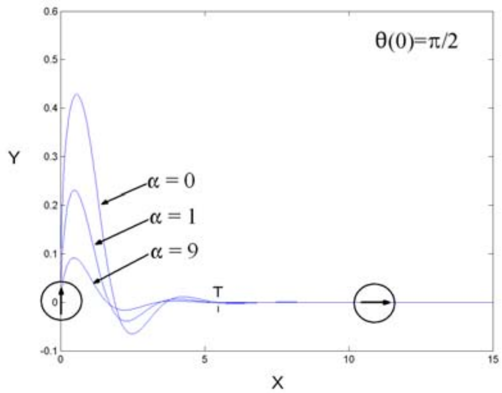

Figure-10: Trajectories from the nonholonomic, kinematic, HPF planner.

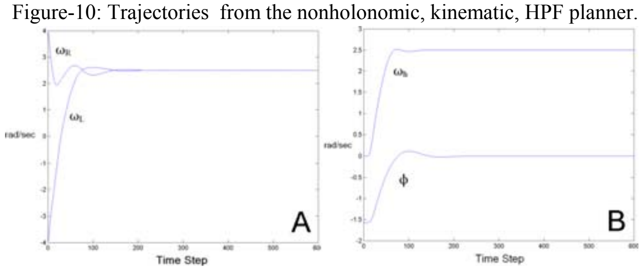

Figure-11: control signals, A-DDR, B-FSR α=9.

In figure-13, the direction sensitive damping is compared to the linear damping case using same coefficients for the planner. As can be seen sensitizing the dampening to direction significantly reduced the overshoot and settling time without compromising the speed of the robot.

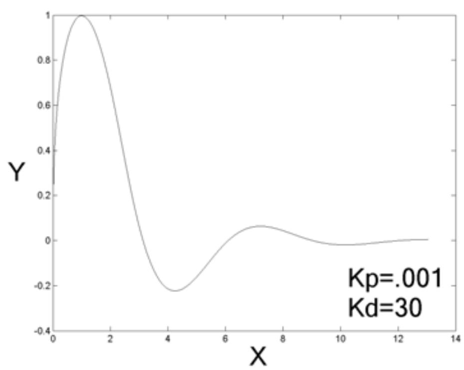

Figure-12: Response of the planner in (13) for different Kp and Kd.

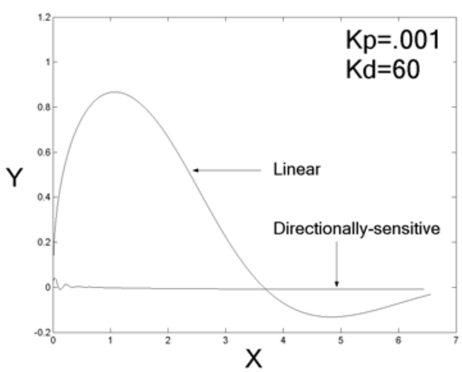

Figure-13: response of the planner in (15) compared to the one in (13).

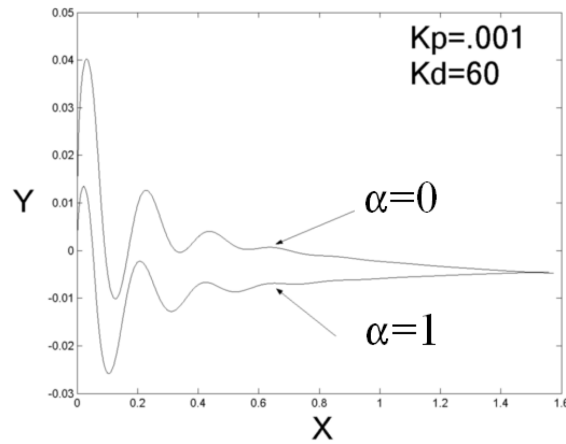

Figure-14: response of the planner in (15) compared to the one in (16).

In figure-14 the direction sensitive controller in (38) simulated for two values of α=0,1. As can be seen the case where α=1 has lower overshoot compared to the case where α=0. Using a K_p=.001 and a K_d=60, The controller in (38) is tested in a cluttered environment. Figure-15 shows the harmonic gradient guidance field that is used to motivate the motion of the robot and the holonomic, kinematic trajectory such a field generates. Figure-16 shows the dynamic trajectory the controller generates for robot as a function of time. As can be seen, the nonholonomic, dynamic trajectory is very close in shape to the holonomic, kinematic trajectory with a satisfactorily smooth orientation profile. The control torques on the right and left wheels of the robot are shown in figure-17. In figure-18 the robustness of the proposed controller in the presence of actuator saturation is tested. The magnitude of the torques (T_R and T_L) is restricted not to exceed Tm:

$$T_m = C \cdot \max(\max_t(Tn_R(t)), \max_t(Tn_L(t))) \qquad (47)$$

where Tn_R and Tn_L are the torques for then non-saturated case, C is a constant representing the percentage saturation. The maximum torque for the non-saturated actuators is equal to .103 N/M. The controller showed remarkable robustness to saturation. The trajectory was virtually unaffected up to 99.8% saturation (i.e. C=.002); a sudden breakdown in performance is observed beyond this limit.

VI. Conclusions

In this paper the ability of the HPF approach to accommodate nonholonomic constraints when planning a trajectory for a robot is demonstrated. This adds a significant improvement to the already existing set of constraints the approach can subject a planning process to in provably-correct manner. It also shows that the wealth of properties harmonic potential fields have (e.g. the goal seeking ability utilized in this paper) is a great asset of the HPF approach and the key to extending the capabilities of the approach. .

Acknowledgment: the author acknowledges KFUPM support

References

[1] J. Schwartz and M. Sharir, "A survey of motion planning and related geometric algorithms," Artif. Intell. J., vol. 37, pp. 157–169, 1988.
[2] Y. Hwang and N. Ahuja, "Gross motion planning," ACM Comput. Surveys,

vol. 24, no. 3, pp. 291–91, Sept. 1992.
[3] R. Aggarwal and G. Leitmann, “A maxmin distance problem,” Trans. ASME, J. Dyn. Syst., Meas. Contr., pp. 155–158, June 1972.
[4] G. Leitmann and J. Skowronski, “Avoidance control,” J. Optim. Theory Appl., vol. 23, no. 4, pp. 581–591, Dec. 1977.
[5] W. Schmitendorf, B. Barmish, and B. Elenbogen, “Guaranteed avoidance control and holding control,” Trans. ASME, J. Dyn. Syst., Meas., Contr., vol. 104, pp. 166–172, June 1982.
[6] S. Masoud A. Masoud, "Constrained Motion Control Using Vector Potential Fields", The IEEE Trans. on Systems, Man, and Cybernetics, Part A: Systems and Humans. May 2000, Vol. 30, No.3, pp.251-272.
[7] C. Langton, “Artificial life,” in Artificial Life SFI Studies in the Science of Complexity, C. Langton, Ed. Reading, MA: Addison-Wesley, 1988, pp. 1–47.
[8] O. Khatib, “Real-time obstacle avoidance for manipulators and mobile robots,” in Proc. IEEE Int. Conf. Robotics Automat., St. Louis, MO, Mar. 25–28, pp. 500–505, 1985.
[9]C. Connolly, R.Weiss, and J. Burns, “Path planning using laplace equation,” in Proc. IEEE Int. Conf. Robotics Automat., Cincinnati, OH, May 13–18, 1990, pp. 2102–2106.
[10]E. Prassler, “Electrical networks and a connectionist approach to pathfinding,” in Connectionism in Perspective, R. Pfeifer, Z. Schreter, F. Fogelman, and L. Steels, Eds. Amsterdam, The Netherlands: Elsevier, North-Holland, 1989, pp. 421–428.
[11]I. Tarassenko and A. Blake, “Analogue computation of collision-free paths,” in Proc. IEEE Int. Conf. Robotics Automat., Sacramento, CA, Apr. 1991, pp. 540–545.
[12]J. Decuyper and D. Keymeulen, “A reactive robot navigation system based on a fluid dynamics metaphor,” in Proc. Parallel Problem Solving From Nature, First Workshop, H. Schwefel and R. Hartmanis, Eds., Dortmund, Germany, Oct. 1–3, 1990, pp. 356–362.
[13] K. Sato, “Collision avoidance in multi-dimensional space using laplace potential,” in Proc. 15th Conf. Robotics Soc. Jpn., 1987, pp. 155–156. 2535-2540.
[14] A. Masoud, Samer A. Masoud, "Evolutionary Action Maps for Navigating a Robot in an Unknown, Multidimensional, Stationary Environment, Part II: Implementation and Results", the 1997 IEEE International Conference on Robotics and Automation, April 21-27, Albuquerque, New Mexico, USA, pp. 2090-2096.
[15] A. Masoud, Samer A. Masoud, "Robot Navigation Using a Pressure Generated Mechanical Stress Field, The Biharmonic Potential Approach", The 1994 IEEE International Conference on Robotics and Automation, May 8-13, 1994 San Diego, California, pp. 124-129.
[16] S. Masoud, Ahmad A. Masoud, " Motion Planning in the Presence of Directional and Obstacle Avoidance Constraints Using Nonlinear Anisotropic, Harmonic Potential Fields: A Physical Metaphor", IEEE Transactions on Systems, Man, & Cybernetics, Part A: systems and humans, Vol 32, No. 6, November 2002, pp. 705-723.
[17] Axler, P. Bourdon, W. Ramey, “Harmonic Function Theory”, Springer, 1992.
[18] D. Koditschek, “Exact robot navigation by means of potential functions: Some topological considerations,” in IEEE Int. Conf. Robotics and Automation, Raleigh, NC, Mar. 1987, pp. 1–6.
[19]D. Koditschek, E. Rimon, “Exact robot navigation using artificial potential functions,” IEEE Trans. Robot. Automat., vol. 8, pp. 501–518, Oct. 1992.
[20] J. Guldner, V. Utkin, “Sliding Mode Control for Gradient Tracking and Robot Navigation Using Artificial Potential Fields”, IEEE Transactions on Robotics and Automation, Vol.
[21] A. Masoud, "A Hybrid, PDE-ODE Control Strategy for Intercepting an Intelligent, Well-Informed Target in a Stationary, Cluttered Environment",Applied Mathematical Sciences, HIKARI Ltd, Vol. 1, 2007, no. 48, 2345-2371..
[22E. Camacho and C. Bordons, “Model Predictive Control”, 2nd ed. NewYork: Springer Verlag, 2004
[23] A. Ben-Israel, G. Thomas, “Generalized Inverses”, Springer-Verlag, 2003.
[24] H. Lutkepohl, “Handbook on Matrices”, Wiley, 1996.
[25] G. Hile, A. Stanoyevitcy, “Gradient Bounds for Harmonic Functions Lipschitz on the Boundary”, Applicable Analysis: An International Journal, Vol. 73 (1-2), July 19, 2007, pp. 101-113.
[26] J. LaSalle, “Some Extensions of Lyapunov’s Second Method”, IRE Trans. Circuit Theory, Vol. CT-7, no.4, pp. 520-527, 1960.

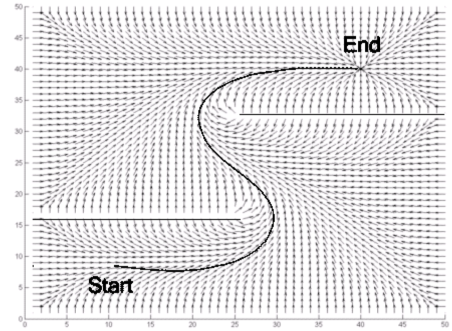

Figure-15: Guidance field and trajectory of a kinematic, holonomic, HPF planner.

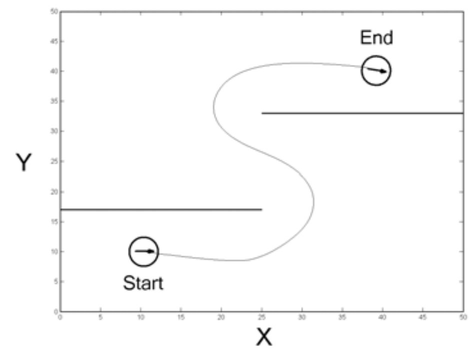

Figure-16: Trajectory and curvature using the planner in (16) and the guidance field in fig. 15.

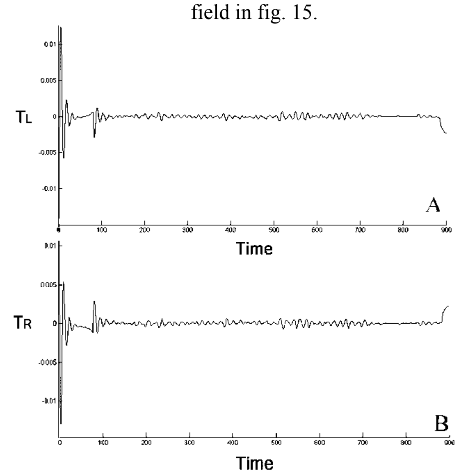

Figure-17: Torque control signals corresponding to fig. 20

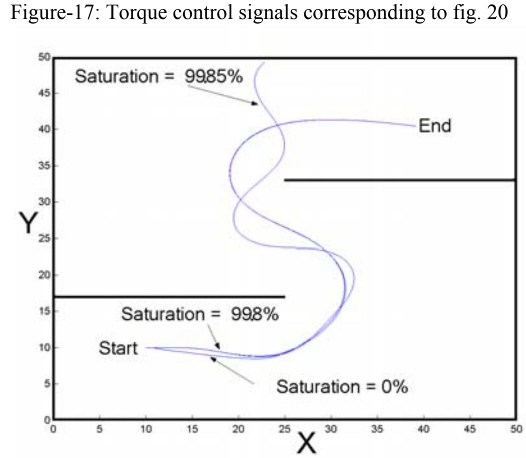

Figure-18: trajectory in the presence of actuator saturation.